


Article

Study on the Mechanical Properties of Corroded Steel Strands at Deflection Angles

Nianchun Deng ^{1,2,*} , Jie Xu ¹, Guochao Zhu ¹ and Zhongqing Han ¹

¹ College of Civil Engineering and Architecture, Guangxi University, Nanning 530004, China; 1910302072@st.gxu.edu.cn (J.X.)

² Guangxi Key Laboratory of Disaster Prevention and Engineering Safety, Nanning 530004, China

* Correspondence: dengnch@gxu.edu.cn

Abstract: The purpose of this study is to investigate the performance changes in steel-stranded hangers under complicated loads in moist or corrosive environments. First of all, corrosion tests were carried over three time periods (360 h, 720 h, 1080 h) on glossy and galvanized steel strands and different levels of corrosion were obtained. Subsequently, tensile tests were carried out on strands with different degrees of corrosion (including no corrosion) at different deflection angles. The test results showed that the ultimate bearing capacity of the uncorroded steel strand at the deflection angle decreased by 21.8%, while the ultimate bearing capacity of the glossy strand with the longest corrosion time decreased by 27.1%. For the same corrosion time, the ultimate bearing capacity of the glossy steel strand decreased at a higher rate than that of the galvanized steel strand. In addition, numerical simulations show that the angle of deflection reduces the ultimate bearing capacity of the steel strand. It is also found that both deflection angle and corrosion pit depth have a positive correlation on the maximum stress of the pit, and that the stress of the pit is highest near the fixed end. This study provides meaningful guidance for the design and maintenance of bridge hangers, which can extend the service life of the hangers.

Keywords: steel strand; corrosion; deflection angle; corrosion pit



Citation: Deng, N.; Xu, J.; Zhu, G.; Han, Z. Study on the Mechanical Properties of Corroded Steel Strands at Deflection Angles. *Buildings* **2023**, *13*, 795. <https://doi.org/10.3390/buildings13030795>

Academic Editor: Krishanu Roy

Received: 20 February 2023

Revised: 12 March 2023

Accepted: 15 March 2023

Published: 17 March 2023



Copyright: © 2023 by the authors. Licensee MDPI, Basel, Switzerland. This article is an open access article distributed under the terms and conditions of the Creative Commons Attribution (CC BY) license (<https://creativecommons.org/licenses/by/4.0/>).

1. Introduction

Seven-wire strands are an important part of various prestressed structures, especially in bridges where they are widely used [1]. The main unit of hangers is the seven-wire strand, which mainly bears the tensile load. In recent years, many half-through and through arch bridges with floating decks have failed due to the breakage of their hangers [2–4], such as the South Gate Bridge (2001), the Peacock River Bridge (2011), and the Nanfang Ao Bridge (2019). The hangers of these bridges all broke at the anchorage and showed obvious signs of corrosion, which was the main cause of failure [5–8]. The technical report of the FHWA presents cases of prestressed strands breaking on existing bridges, and finds that corrosion of prestressed strands occurs mainly at weak locations in the protective jacket, namely the protective jacket's seam at the anchorage. Corrosive substances and air enter through the seams, causing corrosion of the steel strands inside the hangers, a process that occurred at the Sunshine Skyway Bridge and the Niles Channel Bridge [9].

The corrosion of steel strands has become a common problem, so many experts and scholars are conducting research on this phenomenon. Zeng and Gu et al. [10] conducted an experiment on the electrochemically accelerated corrosion of steel strands and on the static load tensioning of precorroded steel strand samples, and concluded that the ultimate strength of a steel strand decreases rapidly with the increase in the degree of corrosion. Chi-Ho Jeon [11] proposed that the degree of corrosion of steel strands depended on three crater structures and introduced a formula for calculating the cross-sectional loss area according to present the crater structure. Moreover, the degree of stretching of corroded

strands was evaluated by tensile tests, and the reduction in the degree of stretching was greater than the reduction in the cross-sectional area. The tensile tests showed that corroded strands or prestressed strands always failed at their minimum cross section [12,13]. The yield strength and elongation of steel strands were reduced by corrosion [14]. Static tensile tests indicated that the deformation capacity of corroded strands was significantly reduced, and the shrinkage of necking tended to disappear as the damage mode changed from plastic fracture to brittle fracture [15,16]. Liu showed through tests that with the increase in the average degree of corrosion, there was a significant change in the cross-sectional area around the corrosion pit and the longitudinal direction of stress concentration [17]. The above tests on corroded strands were conducted in axial tension, but in reality, the mechanical properties of the steel strands are changed, because the steel strands have a certain angular deviation caused by loading and installation.

Corrosion is the main factor causing steel-stranded hangers to break, but in recent years, some scholars believe that the bending deformation generated at the two fixed ends of the hangers is also the cause of their sudden breakage [18–20]. Bending loads can result in variations in the axial force of the space truss [21]. Similarly, the steel strands inside the hangers were stressed by combined axial and bending loads [22]. Bending loads were mainly caused by wind loads or mechanical systems [23]. Steel wire rope is easy to fatigue under bending loads, resulting in the service life of the wire rope being shorted [24]. Diego tested steel strands by applying bending and axial loads. It was found that the maximum stress occurred at the maximum bending moment and that the damage to the strands was controlled by the axial forces [25]. Costello proposed a theory that predicted the stresses in multistranded steel strands under axial, bending, and torsional loads [26]. Hristo I. Ivanov discussed the stresses in multistranded steel strands by testing them under different diameters of wire ropes, structures, levels of friction, and other parameters, and found that bending leads to a reduction in the wire rope's fracture force [27].

According to the above literature, scholars have studied steel strands mainly in terms of the effect of corrosion on their mechanical properties. There are not many studies on steel strand bending, and what studies exist all study the effect of individual factors on steel strands. However, in reality, under loads, the arch ribs are displaced relative to the deck plate and the hangers create a deflection angle [28], as in Figure 1. The deflection angle and corrosion together act on the hangers, causing changes to the mechanical properties of the hangers and shortening their service life. Therefore, it is necessary to investigate the effect of the deflection angle on corroded strands to complement the theoretical and experimental data from related studies and provide scientific guidance for subsequent hanger monitoring. In this paper, tensile tests on steel strands with different degrees of corrosion are carried out at different deflection angles, based on corrosion tests. The finite element model analysis is then used to verify the correctness of the test results and the effect of corrosion pit depth and location on the maximum stress in the steel strand.

In this paper, corrosion tests were carried out over three time periods (360 h, 720 h, and 1080 h) on glossy and galvanized steel strands to obtain different levels of corrosion. Subsequently, anchor plates with different deflection angles were designed and installed on the counterweight frame to perform tension tests. The test results show that the ultimate bearing capacity of uncorroded strands can be reduced by 21.8% at the deflection angle and by 27.1% for corroded strands. The ultimate load bearing capacity of the glossy steel strands decreases more than that of the galvanized steel strands. Secondly, in order to achieve better test accuracy, a new model of "loaded and fixed ends" is proposed. Compared with the simulation results, the model proves to be in good agreement with the test process and close to reality. In addition, a model of a steel strand with corrosion pits is built to analyze the variation in stresses in the depth and location of the pits at the given deflection angles. The study finds that the deflection angle and depth are positively related to the maximum stress of the pit, and that the stress of the pit is greatest near the fixed end. From the above analysis, the deflection angle should be given more attention, especially in the design and maintenance of hangers. Moreover, the new numerical model allows for a better

reproduction of the test process and provides a more realistic approach to the study of steel strands. It is recommended that galvanized steel strands are used in the construction of hangers, which can slow down the rate of corrosion and extend the life of the hangers.

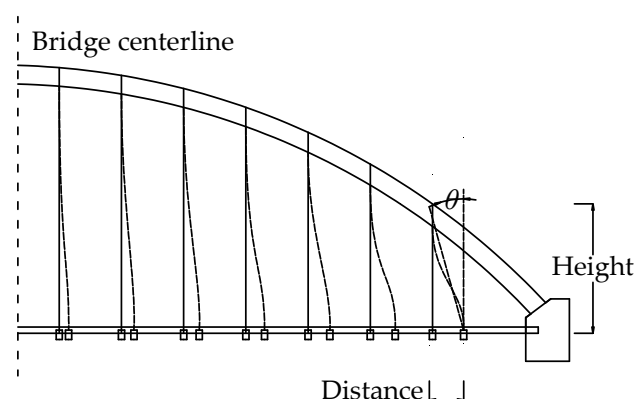


Figure 1. Deflection angle of a hanger.

2. Corrosion Test

2.1. Test Process

The corrosion tests were conducted on glossy seven-wire steel strands and galvanized seven-wire steel strands. The length of all strands is 1900 mm, their diameters are 15.2 mm, and their tensile strength is 1860 MPa. The static test was carried out using the copper salt spray test, and corrosion times of 360 h, 720 h, and 1080 h were used. Glossy steel strands and galvanized steel strands were divided into groups 1 and 2, which included 8 strands for each of the 3 corrosion time periods, for a total of 24 corroded strands per group. The corrosion of steel strands was conducted in a salt spray test chamber, and the influence of temperature, humidity, and other factors on the concentration of the chloride ion field was comprehensively considered. Sodium chloride, cupric chloride dihydrate, glacial acetic acid, and distilled water were used to prepare a salt spray corrosion solution, with its concentration controlled at 0.26 g/L and pH value controlled between 3.1 and 3.3. See Table 1 for the components of the salt spray corrosion solution. The temperature of the salt spray corrosion chamber was controlled at 50 °C, the temperature of the saturated air cylinder was controlled at 65 °C, the pressure was set at 1.0 kg/cm², and the timing function was used to strictly control the time.

Table 1. Chemical composition of salt spray corrosion solution.

Chemical Composition	H ₂ O	NaCl	CuCl ₂ ·2H ₂ O	CH ₃ COOH
Amount/10 L ¹	9437.4 g	500 g	2.6 g	60 mL
Content/10 L ¹	94.37%	5%	0.03%	0.6%

¹ These are contents of each substance per 10 L of solution.

After the completion of the corrosion test, the impurities on the surface of the steel strands due to corrosion were brushed. In order to prevent small impurities and chloride ions from corroding the steel strand matrix, after cleaning, steel strands were immersed in chromic acid solution to completely neutralize the impurities and chloride ions remaining on the surface of the steel strands (Table 2). Then, the strands were washed with clean water, and weighed and recorded after drying.

Table 2. Chromic acid solution.

Chemical Composition	H ₂ O	CrO ₃	AgNO ₃
Amount/1 L ¹	790 mL	200 g	10 g
Content/1 L ¹	79.0%	20.0%	1.0%

¹ These are contents of each substance per 1 L of solution.

2.2. Comparative Analysis of Corrosion Patterns

Corrosion patterns on the steel strands before cleaning are shown in Figures 2 and 3. When the corrosion time is 360 h, yellow-brown substances quickly appear on the surfaces of the glossy steel strands, while the surfaces of the galvanized steel strands are only partially covered in reddish-brown substances, not fully subjected to the corrosion effect. Because the galvanized steel strands contain protective galvanized layers, the corrosion solution reacts with the galvanized layers first, and the corrosive substances do not come into contact with the strand inside. When the corrosion time is 720 h, a large number of yellow-brown substances appear on the surfaces of glossy steel strands, and the corrosion rate is faster. The surfaces of galvanized steel strands still have a large number of red-brown substances, but a small quantity of local yellow-brown substances begin to appear. At this time, the steel strands are into the rapid corrosion stage. When the corrosion time reaches 1080 h, the degree of corrosion of the glossy steel strands is larger, and iron oxide and other black mixtures appear on the strands' surface. The surfaces of galvanized steel strands are covered with reddish-brown substances, the areas of yellow-brown substances are relatively expanded and there is a mixture similar to iron oxide.

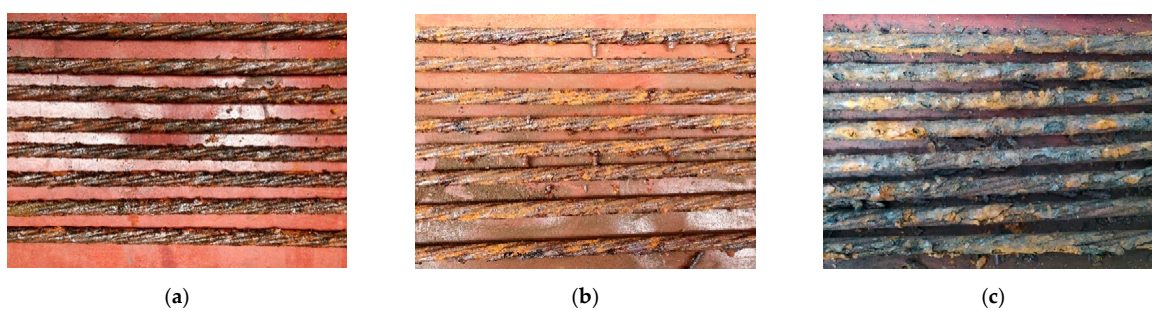


Figure 2. Glossy steel strands under different corrosion times: (a) 360 h, (b) 720 h, (c) 1080 h.

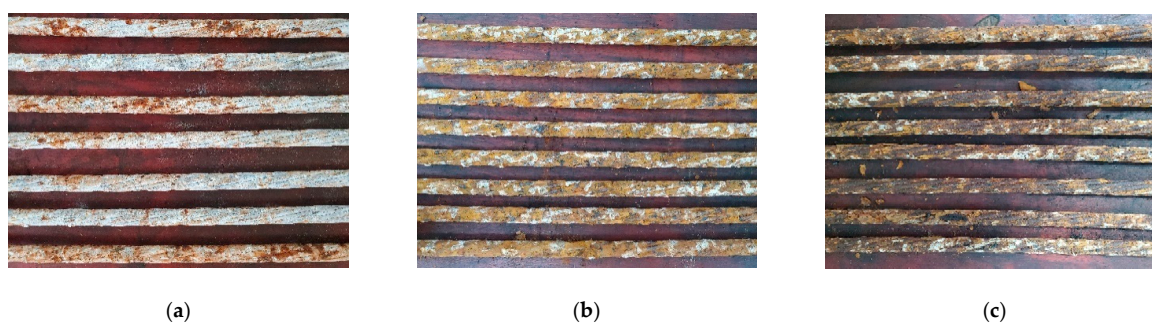


Figure 3. Galvanized steel strands under different corrosion times: (a) 360 h, (b) 720 h, (c) 1080 h.

After a series of cleaning and drying procedures, the corrosion products on the surface of the steel strand are removed, and the patterns of the steel strands are shown in Figures 4 and 5. After 360 h of corrosion, the surfaces of the glossy steel strands are no longer smooth, and there are a lot of smaller corrosion pits. Meanwhile, the galvanized steel strands have white substances on the surface, and the galvanized layers begin to corrode, with small corrosion pits locally. After 720 h of corrosion, the corrosion pits of the glossy steel strands become larger and develop more rapidly; some join together to become larger corrosion pits. The galvanized protective layers of the galvanized steel strands are almost completely corroded, revealing corrosion pits on the inside steel strand; at this time, the corrosion pits are still relatively small. After 1080 h of corrosion, the area of the corrosion pits of glossy steel strands is larger. The development of corrosion pits slows down compared to 720 h, but the depth of the corrosion pits on the steel strand deepens, and the volume of the strand is obviously reduced. The galvanized protective layers of the galvanized steel strands have all been corroded, exposing the internal steel strand, and larger corrosion pits appear on

the inner steel strands. From corrosion tests of the glossy steel strands and galvanized steel strands, corrosion pits develop rapidly in the early stage of corrosion, and gradually expand in depth in the later stage; with the corrosion time prolonged, their degrees of corrosion of both the glossy steel strands or galvanized steel strands are gradually deepened; for galvanized steel strands, because of the galvanized layer of protection, the corrosion solution reacts with the surface zinc first, which can slow down the corrosion rate of the internal steel strand.

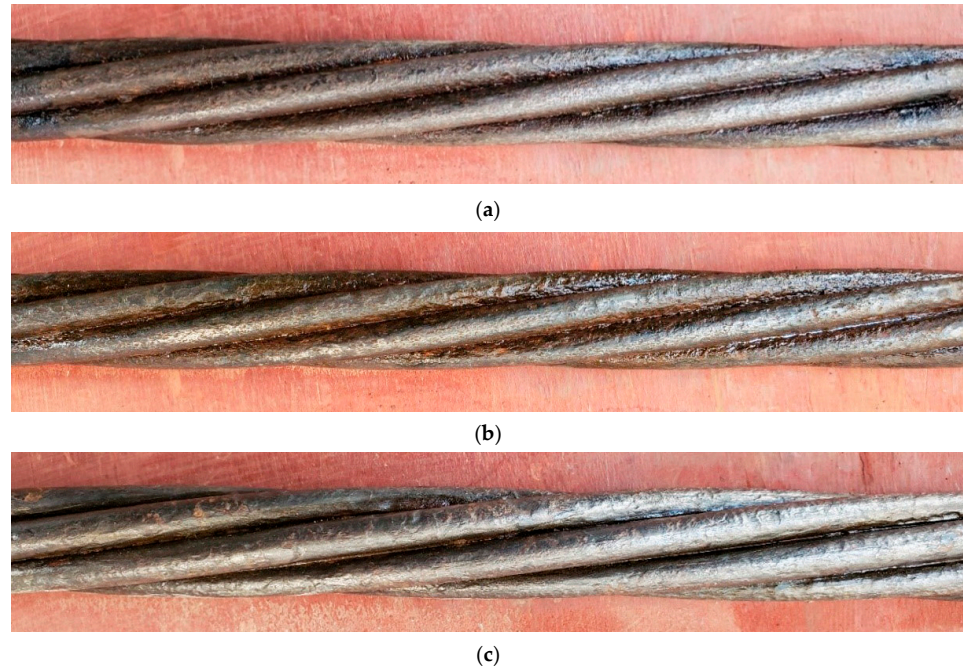


Figure 4. Glossy steel strands after cleaning under different corrosion times: (a) 360 h, (b) 720 h, (c) 1080 h.

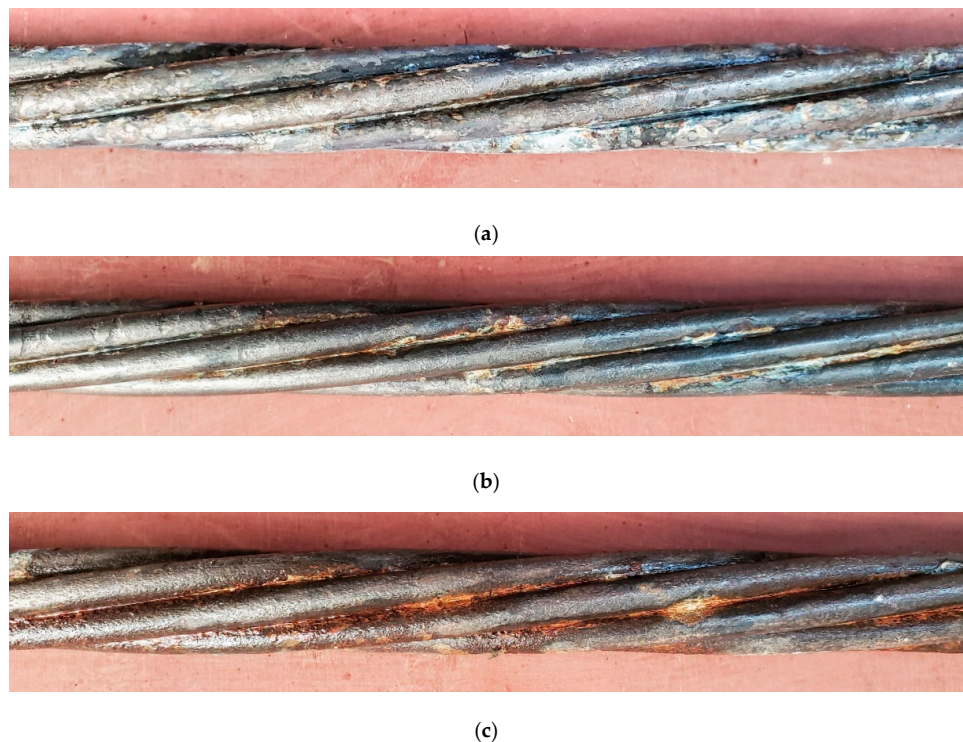


Figure 5. Galvanized steel strand after cleaning under different corrosion times: (a) 360 h, (b) 720 h, (c) 1080 h.

2.3. Degree of Corrosion

For steel strands, the material shape shows no obvious change before and after corrosion, which is not convenient for directly measuring or calculating its defect area. The degree of corrosion is the most important parameter to evaluate the mechanical properties of the tested steel strands. In electrochemistry, this is usually defined by mass loss [29–31], so the weight loss method is used to quantitatively analyze the degree of corrosion of steel strands. The quality of the steel strand before the corrosion test is recorded. After cleaning the impurities and drying the steel strand, the quality of the steel strand after corrosion is recorded again. The degree of corrosion of the steel strand is calculated using Equation (1). To see the degree of corrosion of the steel strand in the unstressed state, see Tables 3 and 4.

$$S = \frac{m_{before} - m_{after}}{m_{before}} \times 100\% \quad (1)$$

where S is the degree of corrosion (%), m_{before} is initial mass (g), and m_{after} is mass after corrosion (g).

Table 3. Degrees of corrosion of glossy steel strands.

Categories	Corrosion Time (h)	Number	Initial Mass (g)	Mass after Corrosion (g)	Degree of Corrosion (%)	Average (%)
Glossy steel strands	360	1-1-1-1	2473.1	2401.0	2.92	2.28
		1-1-1-2	2456.0	2401.3	2.23	
		1-1-2-1	2459.8	2406.2	2.18	
		1-1-2-2	2473.5	2416.7	2.30	
		1-1-3-1	2478.8	2415.5	2.55	
		1-1-3-2	2451.4	2401.5	2.04	
		1-1-4-1	2460.3	2408.4	2.11	
		1-1-4-2	2459.7	2411.7	1.95	
	720	1-2-1-1	2460.0	2378.4	3.32	3.37
		1-2-1-2	2455.4	2367.4	3.58	
		1-2-2-1	2464.7	2377.8	3.53	
		1-2-2-2	2469.3	2387.2	3.32	
		1-2-3-1	2462.7	2376.1	3.52	
		1-2-3-2	2454.5	2375.4	3.22	
		1-2-4-1	2454.0	2371.1	3.38	
		1-2-4-2	2462.1	2386.9	3.05	
	1080	1-3-1-1	2491.0	2376.3	4.60	4.81
		1-3-1-2	2489.6	2379.3	4.43	
		1-3-2-1	2479.3	2364.2	4.64	
		1-3-2-2	2486.3	2346.6	5.62	
		1-3-3-1	2488.2	2360.3	5.14	
		1-3-3-2	2485.3	2378.6	4.29	
		1-3-4-1	2487.4	2371.9	4.64	
		1-3-4-2	2494.3	2366.1	5.14	

It can be seen from Tables 3–5 and Figure 6 that the average degree of corrosion of the glossy steel strands increases with the corrosion time, and the average degree of corrosion of steel strands increases by 0.35% every 100 h of corrosion. The average degree of corrosion of galvanized steel strands also increases with the corrosion time, and the average degree of corrosion of steel strands increases by 0.24% every 100 h of corrosion. However, compared with glossy steel strands, the average degree of corrosion of the galvanized steel strands is lower over the same corrosion time, and the corrosion rate of the galvanized steel strands is also lower than that of the glossy steel strands. In the corrosion time of 360 h, the average degree of corrosion of the glossy steel strands is 2.85 times that of the galvanized steel strands, and after 720 h and 1080 h of corrosion, the average degree of corrosion of the glossy steel strands is 1.98 times and 1.86 times that of the galvanized steel strands,

respectively. With the prolongation of corrosion time, the average degrees of corrosion of the two gradually become similar. Because the glossy steel strands directly react with the corrosion solution in the early stage, the galvanized coating of the galvanized steel strands reacts with the corrosion solution, and the corrosion rates of the two are different. In the later stages of corrosion, the galvanized layers of the galvanized steel strands are corroded off and the internal steel strands are exposed to corrosion, which have a similar corrosion rate as the glossy steel strands. Therefore, the corrosion rate and degree of corrosion of glossy steel strands are greater than those of galvanized steel strands, and the galvanized protective layers can effectively slow down the corrosion rate of the steel strands.

Table 4. Degrees of corrosion of galvanized steel strands.

Categories	Corrosion Time (h)	Number	Initial Mass (g)	Mass after Corrosion (g)	Degree of Corrosion (%)	Average (%)
Galvanized steel strands	360	2-1-1-1	2466.6	2450.5	0.65	0.80
		2-1-1-2	2462.5	2443.4	0.78	
		2-1-2-1	2464.3	2442.4	0.89	
		2-1-2-2	2470.0	2448.2	0.88	
		2-1-3-1	2458.0	2436.9	0.86	
		2-1-3-2	2468.9	2446.4	0.91	
		2-1-4-1	2470.7	2452.2	0.75	
		2-1-4-2	2469.4	2452.2	0.70	
	720	2-2-1-1	2455.9	2416.8	1.59	1.70
		2-2-1-2	2461.7	2418.3	1.76	
		2-2-2-1	2467.1	2421.9	1.83	
		2-2-2-2	2464.7	2433.9	1.25	
		2-2-3-1	2472.2	2424.2	1.94	
		2-2-3-2	2463.2	2427.6	1.45	
		2-2-4-1	2471.3	2425.7	1.85	
		2-2-4-2	2467.7	2420.4	1.92	
	1080	2-3-1-1	2462.5	2395.9	2.70	2.58
		2-3-1-2	2480.6	2407.8	2.93	
		2-3-2-1	2467.5	2401.0	2.70	
		2-3-2-2	2470.7	2401.0	2.82	
		2-3-3-1	2466.7	2408.0	2.38	
		2-3-3-2	2471.9	2412.0	2.42	
		2-3-4-1	2468.9	2410.0	2.39	
		2-3-4-2	2467.0	2410.9	2.27	

Table 5. Significant analysis of the degrees of corrosion of glossy and galvanized steel strands.

Corrosion Time	Categories	Average	Standard Deviation	<i>p</i> -Value
360 h	Glossy steel strands	2.28	0.31	4.22×10^{-9}
	Galvanized steel strands	0.80	0.10	
720 h	Glossy steel strands	3.37	0.18	3.19×10^{-10}
	Galvanized steel strands	1.70	0.25	
1080 h	Glossy steel strands	4.81	0.44	5.46×10^{-9}
	Galvanized steel strands	2.58	0.24	

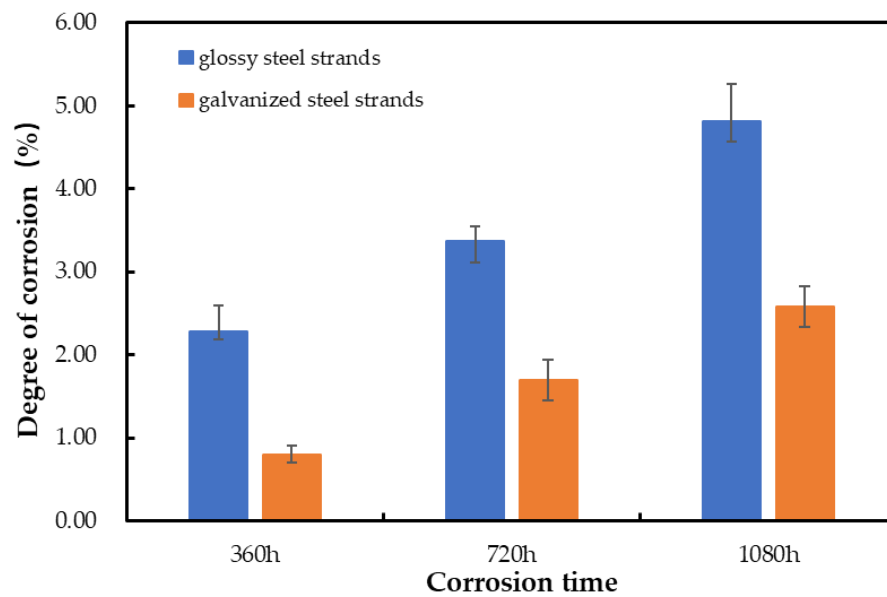


Figure 6. The degrees of corrosion at different times.

3. Tension Test of Steel Strands with Deflection Angles

The deflection angle of the hanger is due to the relative displacement of the two anchorage ends. This deflection angle causes the strand to bend and leads to stress being concentrated on one side of the strand. A deflection angle tensile test was carried out using equipment specifically designed for the test. Figures 7 and 8 show the schemes of the test devices used. In order to realize the deflection angles of the strand, anchor plates with four deflection angles are set: 0 mrad, 10 mrad, 20 mrad, and 30 mrad. A and 1 correspond to the deflection angle of 0 mrad, and the other deflection angles are shown in Figure 9.

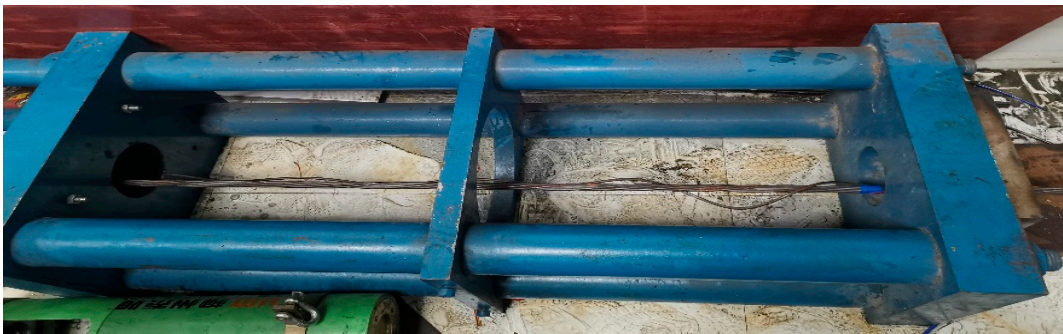


Figure 7. Tension test of steel strands at deflection angles.

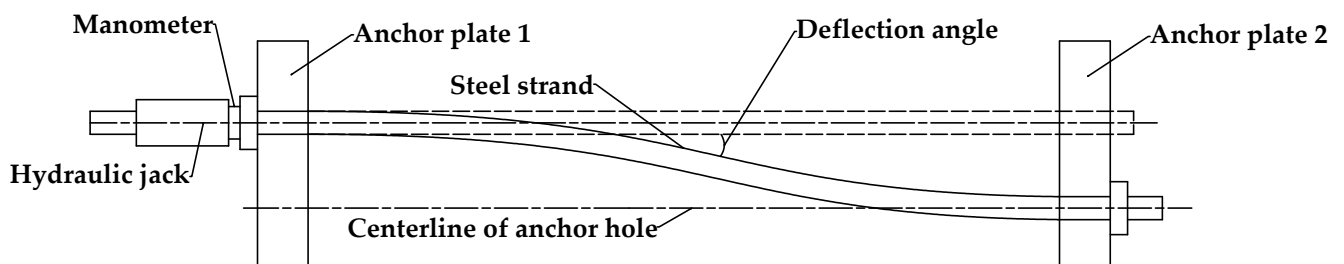


Figure 8. Diagram of the test.

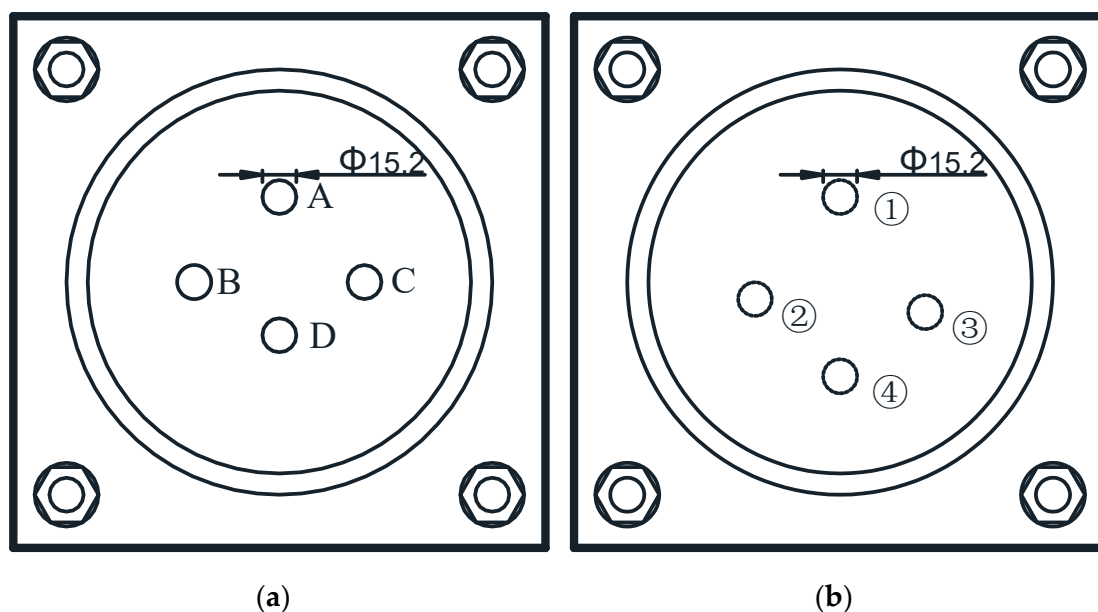


Figure 9. (a) Anchor plate 1; (b) anchor plate 2.

The test objects are steel strands with different degrees of corrosion (including no corrosion), with lengths of 1900 mm, which is about one-quarter of the actual short hanger length. According to Fu [32], if the actual length of the hanger is more than ten times longer than the length of the tested steel strands, the size effect needs to be considered. Therefore, this test does not need to consider the effect of size, and the results are close to the actual scenario. In the test, the bending and tension do not occur simultaneously, while the hanger works under the influence of both tension and bending. However, it was pointed out by Qin [33,34] that the final stress results of the bridge hangers were not influenced by the sequence of the load imposed, but rather the prestress initially applied to the hangers. According to Qin's study, the bending and tensioning of the steel strand in this test does not affect the final results.

Chen discusses sensor deployment positions by means of articulated and fixed boundaries, where the sensors are installed at a certain distance from the boundary [35]. The steel strand is therefore polished clean, and strain gauges are attached 3 cm from the manometer to capture the strain placed on the strand during tension. In the test, one end of the steel strand is anchored and the other end is stretched by a hydraulic jack, as shown in Figures 7 and 8. The test is first loaded at a rate of 10 kN per grade until reaching 90 kN, after which loading is increased at 5 kN per grade. The test stops with the failure of one of the seven wires, and the final tension is recorded.

4. Test Results

4.1. Uncorroded Steel Strand Results

The steel strand enters the yielding stage after the tension reaches 220 kN at a deflection angle of 0 mrad, while at a deflection angle of 30 mrad, the tension enters the yielding stage with only 180 kN of tension. With the increase in the deflection angles, the tensile force required for the steel strand to enter the yielding stage is gradually reduced. After reaching the yielding stage, it is difficult to impose tension until the strand breaks, and the steel strand breaks, as shown in Figures 10 and 11. The tension end of the steel strand shows an unhelix phenomenon, where the steel strand's twisting direction reverses and the strand unwinds. At the fixed end of the steel strand, the first wire breaks. This initial break results in stress being redistributed as well as concentrated, and the rest of the wires break in turn, with the tension end of the steel strand unhelixed, so the fixed end of the steel strand presents a scattered fracture. The bearing capacity of the steel strand is shown in Table 6.

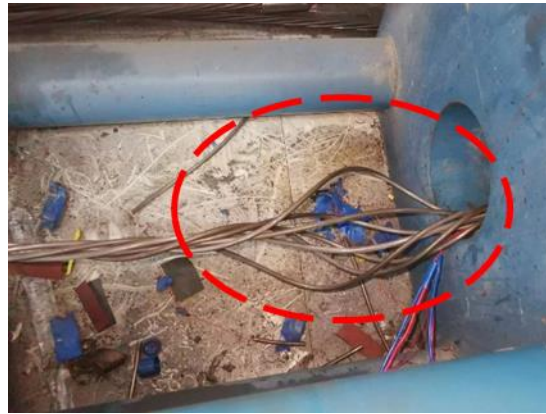


Figure 10. Breakage of strand at the tensile end.



Figure 11. Breakage of strand at the fixed end.

Table 6. Bearing capacity of steel strands with different deflection angles.

Deflection Angle (mrad)	Ultimate Bearing Capacity of Steel Strand (KN)	
	Experimental Results	Average
0	268.9	269.5
	269.5	
	270.1	
10	252.8	251.7
	252.6	
	249.9	
20	225.6	224.6
	224.5	
	223.8	
30	210.4	210.6
	210.6	
	210.8	

The fitting equation is fitted based on the average of the test results, as

$$F = -2.038\theta + 269.67 \quad (2)$$

where F is the bearing capacity (KN) and θ is the deflection angle (mrad).

From Figure 12 and Equation (2), it can be seen that the bearing capacity of the steel strands is negatively linearly related to the deflection angles, i.e., the larger the deflection angle, the smaller the bearing capacity of the steel strand. From Figure 13, the deflection

angle affects the deformation of the steel strand, and the mechanical properties of the steel strand decay as the deflection angle increases. With a deflection angle from 0 mrad to 30 mrad, the bearing capacity of the steel strand decreases by 58.9 KN, a reduction of about 21.8%. For every 1 mrad increase in the deflection angle, the bearing capacity of the strand is reduced by 1.96 KN, a reduction of about 0.73%. When the steel strand is subjected to a deflection angle and tensioning, the steel strand is not only influenced by the tensile force, but also by the bending stress generated by the deflection angle, resulting in a reduction in the bearing capacity of the steel strand. Comparing the steel strand breakage phenomenon, most of their fractures occur at the fixed end. This is the impact of the deflection angle caused by the bending stress, which is the largest at the fixed end.

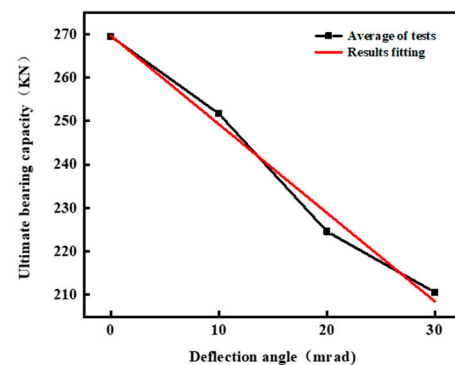


Figure 12. Load capacity of steel strands with different deflection angles.

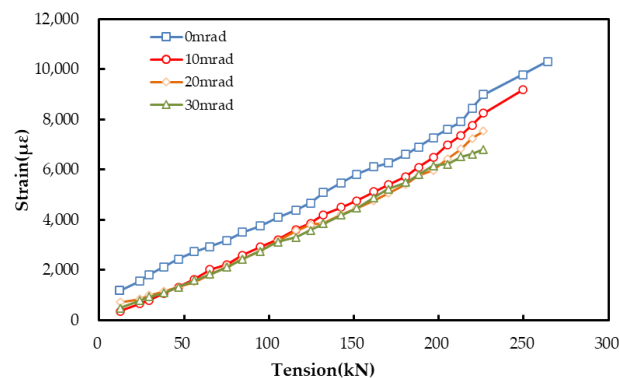


Figure 13. Load–strain curves.

4.2. Corroded Steel Strand Results

Glossy and galvanized steel strands were stressed by static tensile tests under different deflection angles, and the following test results are obtained. The shapes of corrosion damage on the tested strands are as shown in Figure 14. The entire strand appears to have an “exploded” shape, where the wires are scattered around the middle wire in the opposite direction. Compared with the location of damage occurring in the uncorroded strand, damage in the corroded steel strand occurs near the fixed end, where the corrosion level is the largest. Here, the cross-sectional area is reduced by the concentration of tension, so the wire is more likely to enter the yield stage and be pulled off. The uneven degrees of corrosion in various parts of the steel strand leads to uneven force distribution and uneven fracturing.

As shown in Tables 7 and 8, the deflection angles are negatively correlated with the ultimate bearing capacity of both the glossy strand and galvanized strand after the same corrosion time. Specifically, the larger the deflection angle, the smaller the ultimate bearing capacity. For glossy steel strands tested at a deflection angle, when the corrosion times ranged from 360 h to 1080 h, the ultimate bearing capacity decreases from 24.6%, to 27.4%. For galvanized steel strands, the ultimate bearing capacity decreases from 12.9% to 16.1% in the same case.

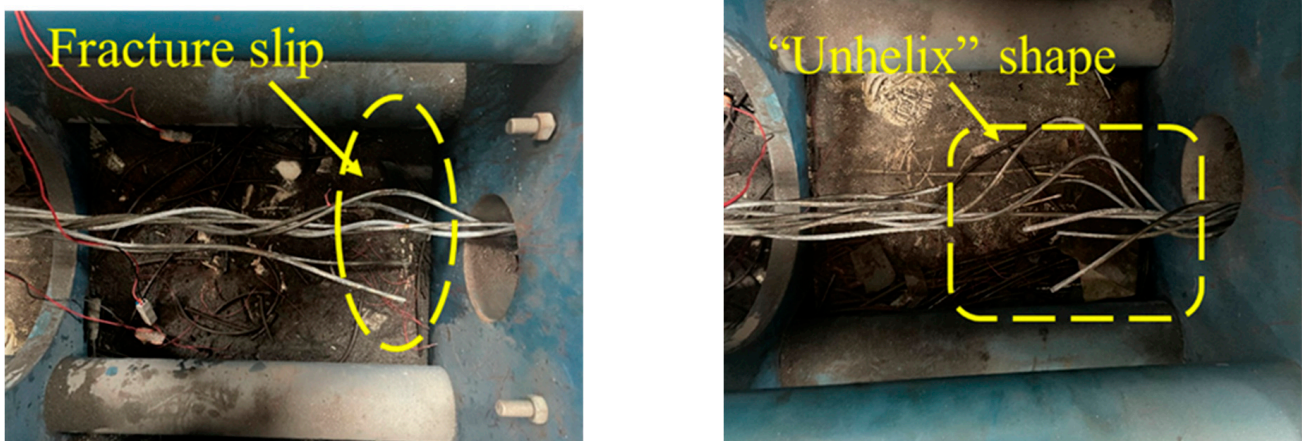


Figure 14. Corrosion strand fracture.

Table 7. Bearing capacity of corroded glossy steel strands with different deflection angles.

Categories	Corrosion Time (h)	Deflection Angles (mrad)	Ultimate Bearing Capacity (KN)	Average Ultimate Bearing Capacity (KN)	
Glossy steel strands	0	0	-	269.5	
		10	-	251.7	
		20	-	224.6	
		30	-	210.6	
	360	0	0	263.6 263.2	263.4
			10	235.5 241.1	238.3
		20	20	210.6 212.9	211.8
			30	199.5 197.4	198.5
	720	0	0	259.0 258.6	258.8
			10	237.4 234.5	236.0
		20	20	202.1 205.6	203.9
			30	186.4 190.7	188.6
	1080	0	0	253.4 249.8	251.6
			10	223.2 221.2	222.2
		20	20	193.4 194.9	194.2
			30	181.5 183.6	182.6

Table 8. Bearing capacity of corroded galvanized steel strands with different deflection angles.

Categories	Corrosion Time (h)	Deflection Angles (mrad)	Ultimate Bearing Capacity (KN)	Average Ultimate Bearing Capacity (KN)
Galvanized steel strands	0	0	260.2 260.2	260.2
		10	254.3 256.8	255.6
		20	243.7 243.9	243.8
		30	236.4 236.5	236.5
	360	0	256.2 259.8	258.0
		10	253.3 253.3	253.3
		20	236.5 235.8	236.2
		30	233.8 215.4	224.6
	720	0	252.5 254.1	253.3
		10	242.5 246.1	244.3
		20	230.6 242.6	236.6
		30	220.4 223.2	221.8
	1080	0	242 250.2	246.1
		10	232.2 232.6	232.4
		20	231.7 221.7	226.7
		30	204.3 208.7	206.5

As shown in Figures 15 and 16, the ultimate bearing capacity decreases with increasing corrosion time at the same deflection angle. For the glossy steel strand, before the corrosion time of 720 h, the reduction rate of the ultimate bearing capacity is faster than after 1080 h. This is because in early stage of the corrosion, the corrosion pits rapidly grow, and the contact area between the steel strand and the corrosion solution expands, which results in a larger corrosion area. In the later stages of corrosion, the corrosion pits are already connected, and the corrosion rate is decreased, which makes the change in the steel strand's degree of corrosion small and also slows down the reduction rate of the ultimate bearing capacity. For the galvanized steel strands, at the corrosion times of 0 and 360 h, the ultimate bearing capacity of the strand at the same deflection angle is not much different. The reason for this is that within 360 h of corrosion, the corrosion solution only reacts with the galvanized layer, so the reaction time is longer. The degree of corrosion of the galvanized steel strand is not deepened, so its ultimate bearing capacity does not change significantly. According to Figure 17 and Table 9, the ultimate bearing capacity of the glossy steel strand is lower than that of galvanized steel strand at the corrosion time of 1080 h. When the deflection angles increase, the difference between the ultimate bearing capacity of the two

strands also increases. In other words, in the same corrosion time, the degree of corrosion of the galvanized steel strand is less than that of the glossy steel strand, which is why its ultimate bearing capacity is superior. The deflection angle and corrosion together have a deeper effect on the ultimate bearing capacity of the glossy steel strand. Hence, galvanized steel strands have a better corrosion resistance and can extend the life of the hangers.

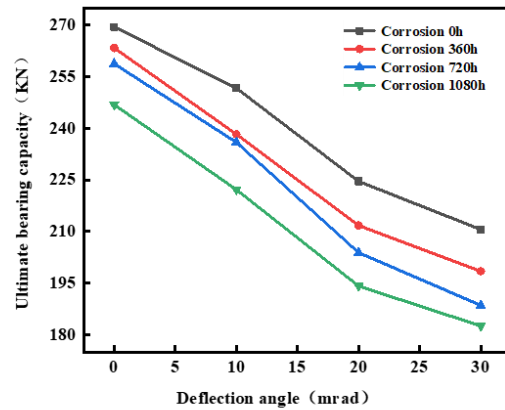


Figure 15. Ultimate bearing capacity of the glossy corroded steel strand.

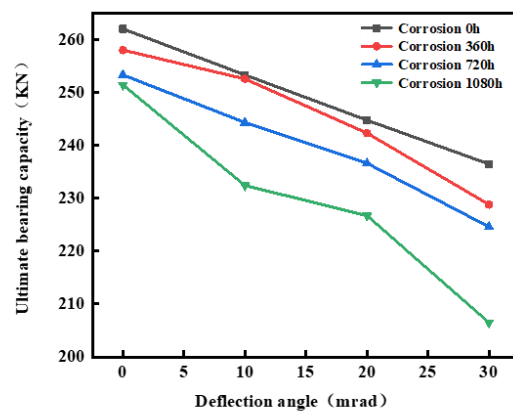


Figure 16. Ultimate bearing capacity of the galvanized corroded steel strand.

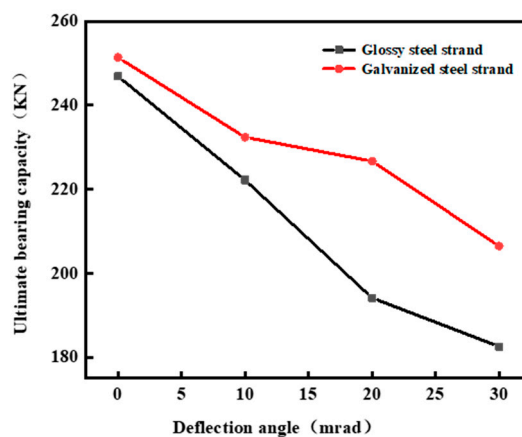


Figure 17. Comparison of steel strands after 1080 h of corrosion.

Table 9. Significance analysis of the deflection angle and corrosion of glossy steel strands.

Source of Difference	Sum of Squares of Deviations	Degree of Freedom	Mean Sum of Squared Deviations	F	<i>p</i> -Value
Deflection angle	20,693.69	3	6897.90	1897.63	1.27×10^{-20}
Corrosion time	2934.46	3	978.15	269.09	6.74×10^{-14}
Deflection angle and Corrosion time	157.65	9	17.52	4.82	0.003
Error	58.16	16	3.63		
Sum	23,843.96	31			

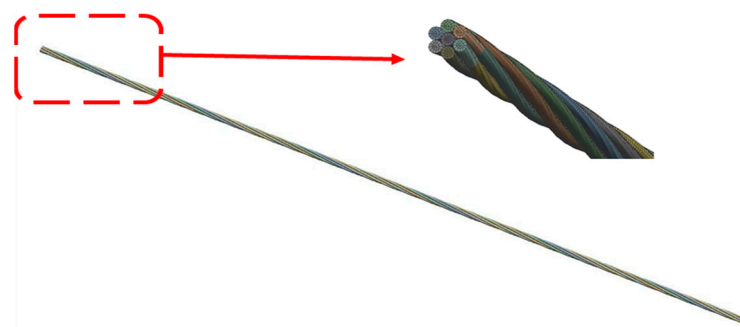
5. Finite Element Simulation

5.1. Effect of Deflection Angle on Steel Strand

Based on the finite element software ANSYS Workbench 2021, a seven-wire steel strand model is established to propose tensile tests with different deflection angles, to obtain more data on the ultimate bearing capacity of steel strands at different deflection angles, and to verify the law of the influence of deflection angles on the ultimate bearing capacity. The geometrical parameters and material properties of the steel strands are shown in Table 10. The SOLID186 unit is used for modeling, and there are 143,587 units. The model length is 1500 mm, and the friction between each wire is 0.16 [36]. The contact mode is body interaction and the solver is MPP [37]. Under the relative balance of calculation accuracy and time, each steel wire is divided into 12 equal parts, based on the divided section along the strand axis using a sweeping method to divide the steel wire. Under this method of division, each microsegment is perpendicular to the wire axis, which is conducive to the tensile deformation of the microsegment along the axis direction. The mesh division diagram is shown in Figure 18.

Table 10. Steel strand geometric parameters and material properties.

Parameter	Value
Diameter (mm)	15.2
Diameter of central wire (mm)	5.2
Diameter of side wire (mm)	5
Twisting distance (mm)	270
Elastic modulus (GPa)	198
Yield strength (MPa)	1860
Poisson's ratio	0.3

**Figure 18.** Model meshing.

The von Mises yield criterion is used to describe the intrinsic structure of the steel strand with respect to the yield criterion and the bilinear isotropic strengthening criterion, as shown in Figure 19.

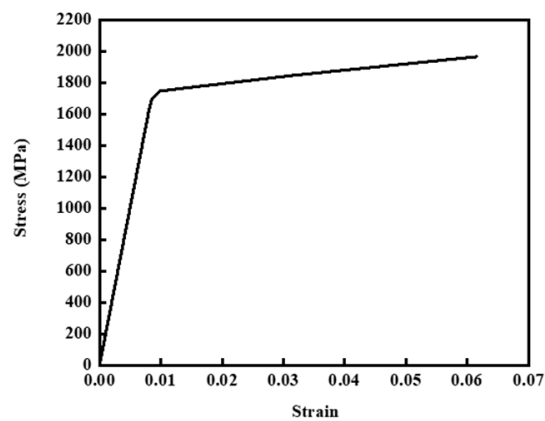


Figure 19. Steel strand stress–strain curve.

One end of the steel strand is fixed by the anchor plate, and the other end is crossed by the hydraulic jack. The fixed end of the steel strand is subject to complete fixation, and the loaded end of the steel strand is free in the axial direction and restrained in the remaining direction, as shown in Figure 8. According to the actual test situation, both ends of the steel strand model are sliced and the nodes of the two loaded sections are coupled with the nodes of the remaining strand sections using a shared topology, so that a strand becomes three parts, that is, the fixed end (anchor end), the loaded end, and the strand body, as shown in Figure 20. Setting the fixed end and the loaded end will effectively simulate the actual conditions of the test, and the loaded end applies a displacement in the Y direction corresponding to the deflection angle to achieve the deflection angle.

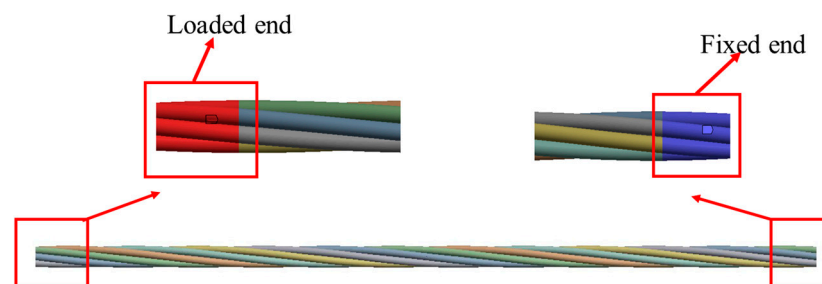


Figure 20. Fixed end and loaded end of the steel strand model.

The deflection angles of 0 mrad, 5 mrad, 10 mrad, 15 mrad, 20 mrad, 25 mrad, and 30 mrad are set. The steel strands under different deflection angles are subjected to axial tension until they fracture; the fracture part of the strand model is as shown in Figure 21. The strand models fracture at both ends, in the same position as the test fracture. The fracture is uneven and similar to the “unhelix” phenomenon in the test. Under the deflection angle and load, the stress of the side wire opposite to the direction of deflection angle is the largest. It is the first to break, resulting in a reduction in the strand’s stiffness. The remaining wires are pulled off one after another and the steel strand is destroyed.

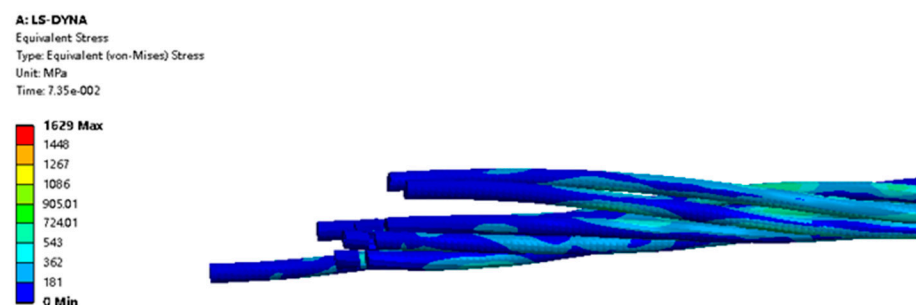


Figure 21. Steel strand model fracture ports.

From Figure 22, it can be concluded that there is a significant weakening of the ultimate bearing capacity of the steel strand at different deflection angles. The ultimate bearing capacity of the steel strand decreases to 212.2 kN at a deflection angle of 30 mrad, which is about 21.7% less than that without deflection. Comparing the test results with the numerical simulation results, the numerical simulation results are mostly higher than the test results. At the deflection angle of 20 mrad, the error between the two is 1.9%, and the overall error is within 5%, indicating that the numerical simulation and the actual test match well. The reason for the errors between the test results and numerical simulation results are as follows: (1) In fact, the mechanical properties of each steel strand are not exactly the same; there are errors in the production process, while the steel strand simulation model is consistent and the geometric parameters and material properties are the same. (2) During the loading process, the steel strands' cross sections are not so smooth, and the steel strands are not subjected to the average surface load in the test, resulting in an uneven force being applied on the wire in the strand; the numerical simulation does not have this problem. (3) The friction coefficient between the wires in the numerical simulation is based on the literature, and the actual steel strands in the friction coefficient between the wires are not the same, resulting in the errors between the two results.

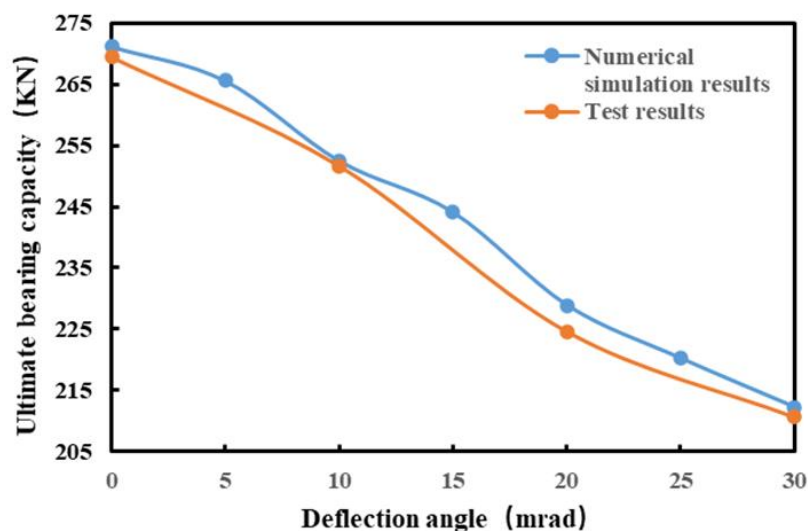


Figure 22. Comparison of the results of the ultimate bearing capacity.

5.2. Analysis of Corrosion Pit Parameters

5.2.1. Depth of Corrosion Pits

According to the relevant literature [38], it is shown that the test piece is defective at the location of the stress concentration, where damage is most likely to occur. For corroded steel strands, the corrosion pits are where the stresses are concentrated. Therefore, researching the stress of each corrosion pit in the strand is unrealistic and meaningless, but can also cause an increase in the calculation. In the case of ensuring the accuracy of the calculation, this paper selected the corrosion pit in the most unfavorable location for simulation.

Based on ANSYS Workbench 2021, this paper calculates the corrosion pits of spheres with radii from 0.2 to 0.6 mm, and the position of the pits is at one-twelfth from the fixed end, as shown in Figure 23. The length of the steel strand model is 540 mm, and the geometric parameters and material properties are shown in Table 10. One end of the corroded steel strand is the fixed end, and the other end is imposed with a surface load of 500 MPa.

In the finite element software analysis, the quality of the mesh is also critical. For accurate and moderate calculations, the steel strand with corrosion pits needs to be encrypted at the level of the corrosion pits. The pit is divided by 0.1 mm, the steel strand around the

pit is divided by 1 mm, and the mesh is divided, as shown in Figure 24. Model-related information is presented in Table 11.

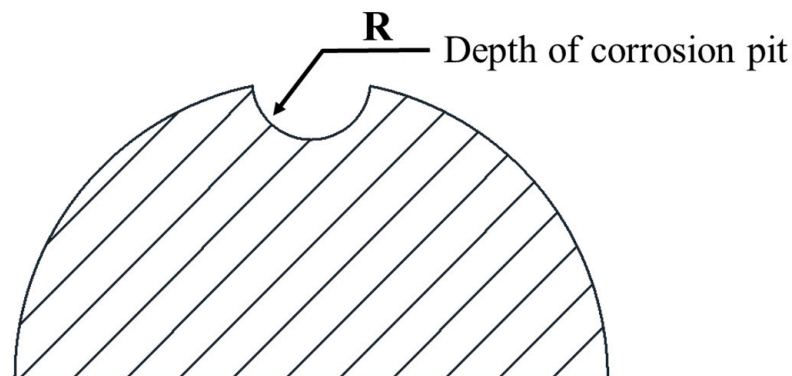


Figure 23. Sphere etching pits.

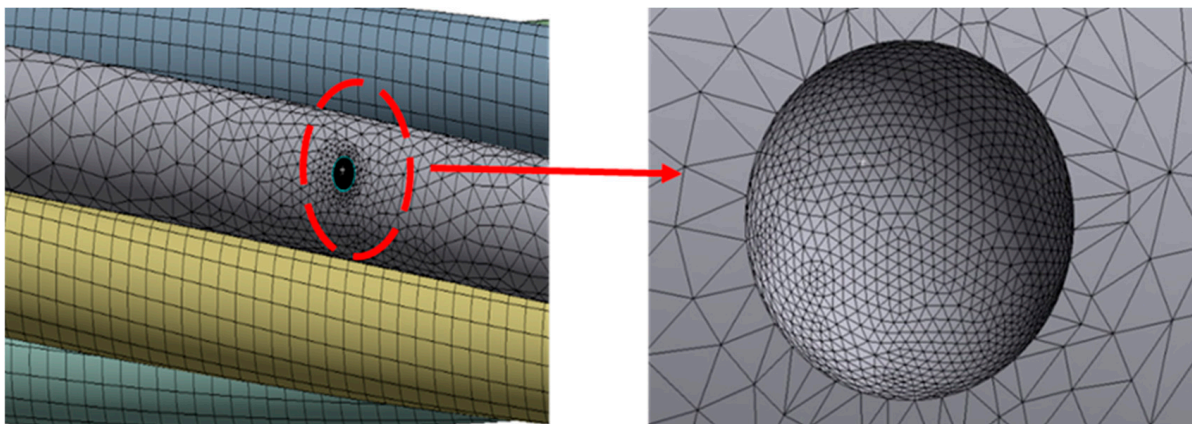


Figure 24. Erosion pit grid diagram.

Table 11. Information on corrosion pit models.

Unit	Number of Units	Corrosion Pit Size	Steel Strand Size
Solid186	122,195	0.1 mm	1 mm

After simulation and analysis, the stress cloud diagram for each deflection angle of the steel strand with a 0.5 mm corrosion pit is shown in Figure 25. The stress distribution of the pit is symmetrically distributed at the center of the circle, and the maximum stress appears in the area near the center. Moreover, the stress is distributed in a belt pattern in the axial direction, and the stress of the pit decreases gradually from the center to both sides. With the increase in the deflection angle, the stress distribution area shows a band distribution, but the maximum stress is gradually increasing. The maximum stress in the pit is 1009.9 MPa when deflection does not occur, and increases to 1907.1 MPa when the deflection angle is 30 mrad. The difference between the two is 897.2 MPa, which is an 88% increase in stress, equivalent to an increase of 29.9 MPa per 1 mrad of deflection. The maximum growth in stress is 161.3 MPa when the deflection angle increases from 0 mrad to 5 mrad, and 128.2 MPa when the deflection angle increases from 25 mrad to 30 mrad. Because plastic transformation occurs at the corrosion pit at this time, the maximum stress growth rate slows down with the increase in the deflection angle.

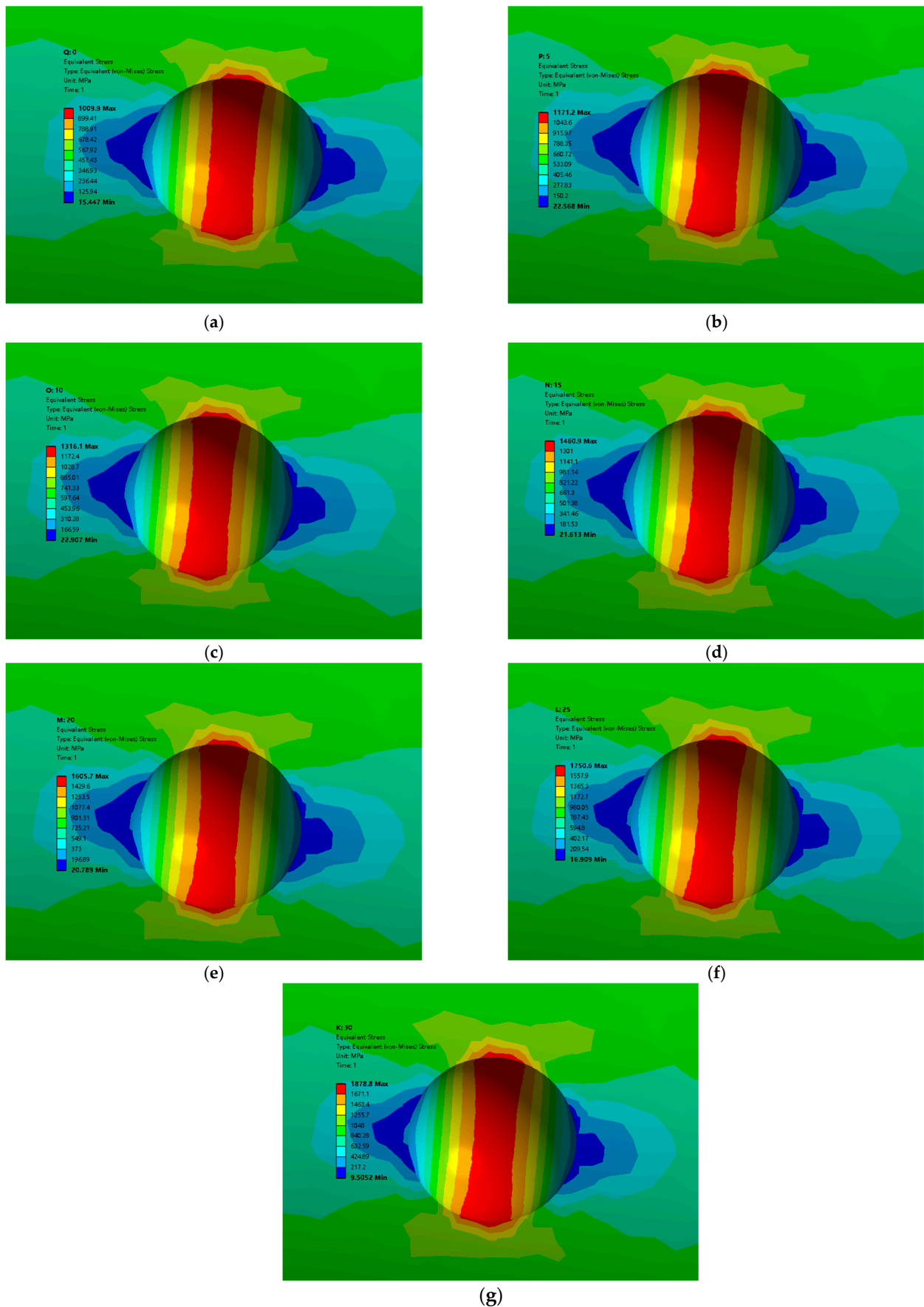


Figure 25. Stress of 0.5 mm corrosion pit: (a) 0 mrad, (b) 5 mrad, (c) 10 mrad, (d) 15 mrad, (e) 20 mrad, (f) 25 mrad, (g) 30 mrad.

In Figures 26 and 27, it can be seen that the deflection angle is linearly and positively correlated with the maximum stress regardless of the corrosion pit depth; that is, the higher the deflection angle, the higher the maximum stress. With the same deflection angle, the depth of the corrosion pit becomes deeper and the maximum stress of the pit becomes larger. At the initial 0.2 mm to 0.4 mm, the maximum stresses in the corrosion pits grow faster, but at 0.4 mm to 0.6 mm, the maximum stresses grow slower. From this situation, it can be concluded that in the early stage of corrosion pit development, shallow corrosion pits can cause rapid increase in stress; when the pits develop to a certain depth, the increase in stress will slow down and gradually enter the yielding stage. The deflection angle would aggravate the corrosion of the steel strand. The effect between the deflection angle and corrosion is mutually promoting, resulting in a reduction in the cross-sectional area of the steel strand and an increase in stress, thus causing the steel strand to break. Therefore, we should focus on the deflection behavior and corrosion of the steel strands and implement strong anticorrosion measures to avoid the failure of the working ability of the steel strand.

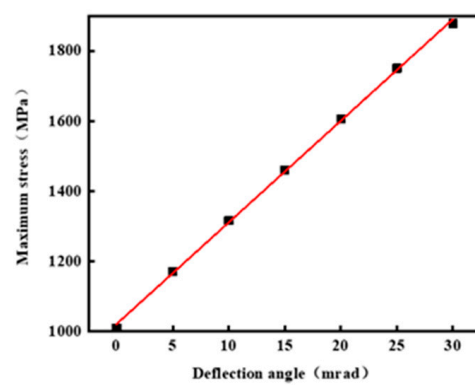


Figure 26. Deflection angle and maximum stress of 0.5 mm corrosion pit.

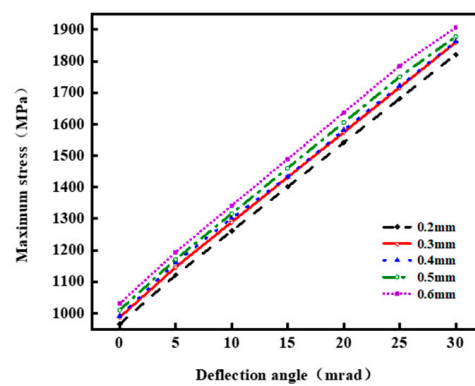


Figure 27. Maximum stress in corrosion pits of different depths.

5.2.2. Location of Corrosion Pits

During the corrosion process, pits are generated at different locations on the steel strand. In ANSYS Workbench 2021, the model's length is 540 mm and the material parameters are listed in Table 10. Deflection angles of 0 to 30 mrad are set, and the depth of the pits is 0.5 mm. One end of the steel strand is the fixed end and one end is surface-loaded at 500 MPa. The pits are located at 1/12, 1/6, 1/3, and 1/2 of the strand (that is, 45 mm, 90 mm, 180 mm, and 270 mm from the fixed end, respectively).

Figure 28 shows that the maximum stress increases with the increase in the deflection angle at 1/12, 1/6, and 1/3. However, the maximum stress in the corrosion pit at 1/2 is negatively linearly related to the deflection angle, and the maximum stress decreases instead when the deflection angle increases. When deflection does not occur, the maximum stress at each position is around 1000 MPa, and there is no significant difference. However, when the steel strand is deflected, the maximum stresses are gradually separated, and at

the same deflection angle, the maximum stresses at 1/12 are all higher than the maximum stresses at the other positions, which indicates that the closer the fixed end is, the higher its maximum stress is. Figure 29 shows that at the deflection angle of 15 mrad, the corrosion pit is located at 1/2 of the steel strand and the maximum stress is not a complete band distribution, after which the maximum stress appears at the fixed end and the maximum stress at the corrosion pit does not change in an obvious way. From the above observations and data, the stress of the corrosion pit near the fixed end is the largest. Due to the bending moment generated by the steel strand with the deflection angle, the bending moment produces a higher bending stress near the fixed end, causing the stress of the corrosion pit also the largest at this end. In reality, deflection also occurs in the working conditions of hangers made of steel strands, and corrosive substances can come into contact with the internal structure. Hanger accidents usually occur at the fixed end. This illustrates that when the steel strands or hangers are corroded, the deflection angle will generate greater stress at the anchorage and aggravate the degree of corrosion.

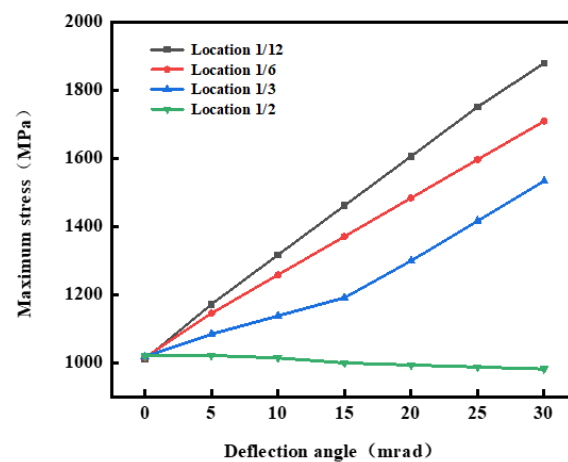


Figure 28. Relationship between deflection angle and maximum stress at different positions.

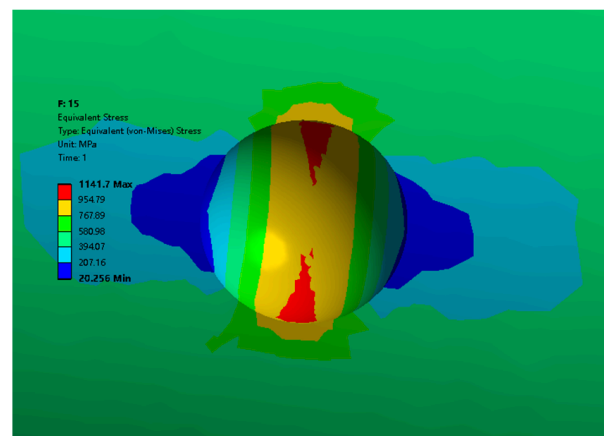


Figure 29. Stress diagram at 15 mrad and 1/2 position.

6. Conclusions

In this paper, a series of tensile tests on steel strands at different deflection angles was carried out on the basis of corrosion tests. A new steel strand model is proposed that is more closely matched to the test procedure. According to the finite element analysis of the steel strands with corrosion pits, the variation in the maximum stress in the corroded steel strands is caused by the depth and position of the pits at the deflection angles. This paper studies the deflection angle and corrosion, without considering fatigue. In the future, the effects of the deflection angle, corrosion, and fatigue on the strand hangers will be further

investigated, and a new method of monitoring stress changes at the anchored end of the hanger will be proposed. The following conclusions are drawn:

1. The deflection angle is negatively linearly related to the ultimate bearing capacity of the steel strand, which means that the larger the deflection angle is, the lower the ultimate bearing capacity of the steel strand. For every 1 mrad increase in the deflection angle, the ultimate bearing capacity decreases by 0.73%. With the deflection angle, the steel strand assumes an “unhelix” shape at the loaded end. The deflection angle leads to a bending moment, resulting in additional bending stress on the fixed end of the steel strand, hence the fixed end of the steel strand is mostly broken.
2. With the increase in corrosion time, the degree of corrosion of the steel strands increases, and the corrosion rate of steel strands is faster in the early stage of corrosion than the later stage. In the same corrosion time, the degree of corrosion of glossy steel strands is much greater than galvanized steel strands, and the corrosion rate is faster than galvanized steel strands.
3. Under the same degree of corrosion, the ultimate bearing capacities of the glossy steel strand and galvanized steel strand gradually decrease with the increase in the deflection angle. At the same deflection angle, the ultimate bearing capacities of the glossy steel strand and galvanized steel strand decrease with the increase in corrosion. In the 0–360 h corrosion time, there is not much difference in the ultimate bearing capacity and corrosion of the galvanized steel strand. This is because in 360 h, only the galvanized layer of the galvanized steel strand is corroded, and the internal steel wire is not really affected, so its ultimate bearing capacity is basically unaffected as well.
4. In the FE model simulation analysis, the maximum stress appears in the central zone of the corrosion pits. The stress band forms in the central part of the pit and decreases in layers towards the sides. At the same depth, the higher the deflection angle, the higher the maximum stress. For the same deflection angle, the pit is deeper, and the maximum stress is higher. The stress distribution is different when the pit is loaded at different positions. The larger the deflection angle is for a corrosion pit at 1/2 of the steel strand, the higher the maximum stress may appear at the fixed end. With deflection angle, as the pit is closer to the fixed end, the higher the maximum stress is.

Author Contributions: N.D. designed the experiments and funded the paper. J.X. and G.Z. conducted the experiments. J.X. analyzed the data and wrote the paper. Z.H. audited the content. All authors have read and agreed to the published version of the manuscript.

Funding: This research was funded by the National Natural Science Foundation of China (grant no. 51868006, 52268048) and the Guangxi Science and Technology Major Project of China (Gui Ke AA22068066).

Data Availability Statement: The data that support the research can be obtained from the corresponding author upon reasonable request.

Conflicts of Interest: The authors declare no conflict of interest.

References

1. Yu, Y.J. *Semi-Refined Finite Element Model of Cable and Its Application on Bending Behavior and Wire Break*; Tianjin University: Tianjin, China, 2015.
2. Liu, J.F.; Li, Y.B.; Zhang, Q.W. Mechanical behavior of damaged strand suspender with asymmetric broken wires in arch bridges. *J. Tongji Univ.* **2019**, *47*, 451–457.
3. Zhong, S.T. *The Concrete-Filled Steel Tubular Structures*; Tsinghua University Press: Beijing, China, 2003.
4. He, W.; Chen, H. Characteristics and Related Research of through and Half through Arch Bridges in China. *Appl. Mech. Mater.* **2014**, *488–489*, 509–512.
5. Li, Y.; Lv, D.G.; Sheng, H.F. Fatigue Reliability Analysis of the Stay Cables of Cable-Stayed Bridge under Combined Loads of Stochastic Traffic and Wind. *Key Eng. Mater.* **2011**, *456*, 23–35.
6. Qu, Y.; Zhang, H.; Zhao, R.; Liao, L.; Zhou, Y. Research on the Method of Predicting Corrosion width of Cables Based on the Spontaneous Magnetic Flux Leakage. *Materials* **2019**, *12*, 2154. [[CrossRef](#)]

7. Winkler, J.; Georgakis, C.; Fischer, G.; Wood, S.; Ghannoum, W. Structural Response of a Multi-Strand Stay Cable to Cyclic Bending Load. *Struct. Eng. Int.* **2015**, *25*, 141–150. [[CrossRef](#)]
8. Sophianopoulos, D.S.; Michaltsos, G.T.; Cholevas, H.I. Static and dynamic responses of suspended arch bridges due to failure of cables. *Arch. Appl. Mech.* **2019**, *89*, 2281–2312. [[CrossRef](#)]
9. Trejo, D.; Hueste, M.B.D.; Gardoni, P.; Pillai, R.G.; Reinschmidt, K.; Im, S.B.; Kataria, S.; Hurlebaus, S.; Gamble, M.; Ngo, T.T. *Effect of Voids in Grouted Post-Tensioned Concrete Bridge Construction: Electrochemical Testing and Reliability Assessment*; Texas Transportation Institute: Austin, TX, USA, 2009.
10. Zeng, Y.H.; Gu, X.L.; Zhang, W.P.; Huang, Q.H. Study on Mechanical Properties of Corroded Prestressed Tendons. *J. Build. Mater.* **2010**, *13*, 169–174+209.
11. Jeon, C.-H.; Lee, J.-B.; Lon, S.; Shim, C.-S. Equivalent material model of corroded prestressing steel strand. *J. Mater. Res. Technol.-JMRT* **2019**, *8*, 2450–2460. [[CrossRef](#)]
12. Zhu, W.; François, R.; Poon, C.S.; Dai, J. Influences of corrosion degree and corrosion morphology on the ductility of steel reinforcement. *Constr. Build. Mater.* **2017**, *148*, 297–306. [[CrossRef](#)]
13. Zhu, W.; François, R.; Cleland, D.; Coronelli, D. Failure mode transitions of corroded deep beams exposed to marine environment for long period. *Eng. Struct.* **2015**, *96*, 66–77. [[CrossRef](#)]
14. Apostolopoulos, C.A.; Demis, S.; Papadakis, V.G. Chloride-induced corrosion of steel reinforcement—Mechanical performance and pit depth analysis. *Constr. Build. Mater.* **2013**, *38*, 139–146. [[CrossRef](#)]
15. Zhu, W.; François, R. Experimental investigation of the relationships between residual cross-section shapes and the ductility of corroded bars. *Constr. Build. Mater.* **2014**, *69*, 335–345. [[CrossRef](#)]
16. Imperatore, S.; Rinaldi, Z.; Drago, C. Degradation relationships for the mechanical properties of corroded steel rebars. *Constr. Build. Mater.* **2017**, *148*, 219–230. [[CrossRef](#)]
17. Liu, X.; Zhang, W.; Gu, X.; Ye, Z. Probability distribution model of stress impact factor for corrosion pits of high-strength prestressing wires. *Eng. Struct.* **2012**, *230*, 111686. [[CrossRef](#)]
18. Wang, D.; Yang, Q.; Liu, Y. Analysis of cable bending stiffness effect on test accuracy of anchor span tension for long-span suspension bridge. *J. Comput. Mech.* **2015**, *32*, 174–179.
19. Zheng, W. Bending Stress of Stay Cables of Cable-stayed Bridges and Probe into Control Countermeasures. *Technol. Highw. Transp.* **2013**, *5*, 90–93.
20. Huang, B.; Li, Y.; Zhu, L.; Zhang, W. Effects of Towers' Random Sectional Bending Stiffness on Dynamic Characteristics of Large-Span Cable-Stayed Bridge. *J. Southwest Jiaotong Univ.* **2014**, *49*, 202–207.
21. Bonopera, M.; Chang, K.C.; Chen, C.C.; Lin, T.K.; Tullini, N. Bending tests for the structural safety assessment of space truss members. *Int. J. Space Struct.* **2018**, *33*, 138–149. [[CrossRef](#)]
22. Gimsing, N.J.; Georgakis, C.T. *Cable Supported Bridges Concept and Design*, 3rd ed.; Wiley Press: West Sussex, UK, 2012; pp. 148–156.
23. Peterka, P.; Krešák, J.; Kropuch, S.; Fedorko, G.; Molnar, V.; Vojtko, M. Failure analysis of hoisting steel wire rope. *Eng. Fail. Anal.* **2014**, *45*, 96–105. [[CrossRef](#)]
24. Pal, U.; Mukhopadhyay, G.; Sharma, A.; Bhattacharya, S. Failure analysis of wire rope of ladle crane in steel making shop. *Int. J. Fatigue* **2018**, *116*, 149–155. [[CrossRef](#)]
25. Erena, D.; Vázquez Valeo, J.; Navarro, C.; Domínguez, J. Fatigue and fracture analysis of a seven-wire stainless steel strand under axial and bending loads. *Fatigue Fract. Eng. Mater. Struct.* **2019**, *43*, 149–161. [[CrossRef](#)]
26. Costello, G.A. Stresses in multilayered cables. *J. Energy Resour. Technol.* **1983**, *105*, 337–340. [[CrossRef](#)]
27. Ivanov, H.I.; Ermolaeva, N.S.; Breukels, J.; de Jong, B.C. Effect of bending on steel wire rope sling breaking load: Modelling and experimental insights. *Eng. Fail. Anal.* **2020**, *116*, 766–767. [[CrossRef](#)]
28. Zhou, Y.; Deng, N.; Yang, T. A Study on the Strength and Fatigue Properties of Seven-Wire Strands in Hangers under Lateral Bending. *Appl. Sci.* **2020**, *10*, 2160–2182. [[CrossRef](#)]
29. Wu, X.; Li, H. Effect of strain level on corrosion of prestressing steel strands. In Proceedings of the International Association for Bridge and Structural Engineering, Guangzhou, China, 8–12 May 2016; pp. 292–299.
30. Xia, J.; Jin, W.L.; Zhao, Y.X.; Li, L.Y. Mechanical performance of corroded steel bars in concrete. *Struct. Build.* **2013**, *166*, 235–246. [[CrossRef](#)]
31. Rinaldi, Z.; Imperatore, S.; Valente, C. Experimental evaluation of the flexural behavior of corroded P/C beams. *Constr. Build. Mater.* **2010**, *24*, 2267–2278. [[CrossRef](#)]
32. Fu, G.L.; Huang, Y.P.; Xu, M. Research on Actual Entire Curve Testing Method of Steel Strand Stretching. *Eng. Test.* **2006**, *46*, 31–34.
33. Qin, S.Q. Unstressed State Control Method for Bridges Constructed in Stages. *Bridge Const.* **2008**, *1*, 14.
34. Yuan, R.N.; Qin, S.Q. Application of Unstressed Stage Method to Construction of Steel Strand Stay Cable. *Bridge Const.* **2012**, *42*, 75–79.
35. Chen, C.C.; Wu, W.H.; Chen, S.Y.; Lai, G. A novel tension estimation approach for elastic cables by elimination of complex boundary condition effects employing mode shape functions. *Eng. Struct.* **2018**, *166*, 152–166. [[CrossRef](#)]
36. Abdullah, A.B.M.; Rice, J.A.; Hamilton, H.R.; Consolazio, G.R. Experimental and Numerical Evaluation of Unbonded Posttensioning Tendons Subjected to Wire Breaks. *J. Bridge Eng.* **2016**, *21*, 04016066. [[CrossRef](#)]

37. Wang, X.M. *ANSYS Numerical Analysis of Engineering Structures*, 1st ed.; People's Traffic Press: Beijing, China, 2019; pp. 265–266.
38. Xu, K.K.; Chen, R.; Peng, A.H.; Huang, W.Y.; Cao, Y.M. Distribution Characteristics of Pits Size of Steel Strands Corroded by Simulated Acid Rain. *J. East China Jiaotong Univ.* **2021**, *38*, 22–28.

Disclaimer/Publisher's Note: The statements, opinions and data contained in all publications are solely those of the individual author(s) and contributor(s) and not of MDPI and/or the editor(s). MDPI and/or the editor(s) disclaim responsibility for any injury to people or property resulting from any ideas, methods, instructions or products referred to in the content.